Pergamon

Int. J. Heat Mass Transfer. Vol. 38, No. 11, pp. 1957–1973, 1995

0017-9310/95 $9.50+0.00

0017-9310(94)00329-7

A numerical and experimental study of three-dimensional transport in the channel of an extruder for polymeric materials

T. SASTROHARTONO,† Y. JALURIA,‡ M. ESSEGHIR§ and V. SERNAS

Department of Mechanical and Aerospace Engineering, Rutgers, The State University of New Jersey, New Brunswick, NJ 08903, U.S.A.

(*Received* 24 *May* 1994 *and in final form* 15 *October* 1994)

Abstract—A numerical study of the three-dimensional flow and heat transfer in a single-screw extruder for polymeric materials such as plastics is carried out. The mathematical model is considerably simplified by conceptually unwrapping the channel and fixing the coordinate system to the rotating screw. Despite this simplification, strong property variations, particularly in the viscosity, complicated cross-sections employed in practical systems, large viscous dissipation effects and non-Newtonian nature of typical extruded materials make the problem a very difficult one to model numerically. Therefore, the transport processes in the extruder channel are simulated by means of a finite-element scheme which employs marching in the down-channel direction. The cross-section of the channel is taken as the commonly used rectangular or self-wiping profiles. An experimental study is also carried out using Newtonian and non-Newtonian fluids in order to provide data for the validation of the numerical model and also to quantify possible recirculation in the channel. Numerical results are presented on the temperature and velocity fields, resulting shear effects, pressure rise, heat transfer rates and viscous heating. The comparisons with experimental results indicate good agreement. A strong recirculating flow is found to arise over the cross-section of the channel. It is shown that a three-dimensional modeling of the process is necessary to capture the effects of recirculation in the channel. However, the marching procedure considerably simplifies the model as well as the inclusion of property changes and chemical reactions.

1. INTRODUCTION

Extrusion is one of the most important manufacturing methods in many industries. This process is particularly useful when thermal and/or mechanical means are required to obtain a uniformly processed product in a continuous operation. The extrusion process for plastic materials usually includes the following stages: feeding, conveying, plasticizing, homogenizing and pressurizing [1]. These processes take place within a special reactor consisting of one or more screws rotating inside a barrel, usually referred to as single, twin or multiscrew extruders. The cross-sectional shape of the product is obtained by pushing the molten material through a die. In order to obtain desired product quality and characteristics, a given set of operating parameters has to be maintained at certain values, for a particular design of the extruder. The main operating parameters are the screw rotational speed and the barrel temperature, while the extruder design parameters are screw diameter, screw profile and length [1]. The desired temperature level at the barrel is maintained by electrical heating, by using a hot fluid, and/or by cooling of the barrel.

The extrusion technique has been increasingly used in many industries, such as those related to pharmaceuticals, food and polymers. Extensive experimental and numerical studies have been carried out for the purpose of understanding the transport phenomena in the extrusion process, resulting in much scientific knowledge, primarily for single-screw extruders. Nevertheless, the design and operation of the extruder are still more art than science. The first published analysis for simulation of the flow in a single-screw extruder is attributed to Rowell and Finlayson [2]. In this analysis, the screw channel is held stationary while the barrel is considered to move in a direction opposite to that of the actual screw rotation. In one of the pioneering studies on the flow in a single-screw extruder, Griffith [3] solved for the fully developed flow of an incompressible, power-law, fluid in a screw extruder. The velocity and the temperature profiles are essentially the same as those in a channel of infinite width and length. The effects of curvature and leakage, across the flights, were also ignored. Zamodits and Pearson [4] obtained numerical solutions for a fully developed, two-dimensional non-Newtonian flow of polymer melts in infinitely wide rectangular screw channels, taking into account the effect of transverse flow and of a superimposed steady

† Present address: Gedung BPP Teknologi, Jakarta, Indonesia.

‡ Author to whom correspondence should be addressed.

§ Present address: Polymer Processing Institute, Stevens Institute of Technology, Hoboken, NJ 07030, U.S.A.

NOMENCLATURE

C_p	specific heat at constant pressure	T_i	inlet temperature
D_b	diameter of the barrel	t	screw pitch
e	width of the screw flight tip	u	velocity component in the x direction
g	gap between the screw flight tip and the barrel surface	V_b	barrel velocity
		V_{bx}	barrel velocity component in the x direction
H	maximum depth of the screw channel	V_{bz}	barrel velocity component in the z direction
h	heat transfer coefficient		
k	thermal conductivity	**V**	velocity vector
LDPE	low-density-poly-ethylene	v	velocity component in the y direction
l_a	axial distance	W	maximum width of the screw channel
N	screw rotational speed	w	velocity component in the z direction
Nu	Nusselt number	x	x coordinate
n	power-law index	y	y coordinate
p	pressure	z	z coordinate.
$\bar{p}$	pressure in down channel direction		
Pr	Prandtl number, $Pr = \mu C_p/k$	Greek symbols	
Q	volume flow rate	$\dot{\gamma}$	shear rate
q	heat flux	μ	viscosity
q_v	normalized volume flow rate	ρ	density
$\dot{Q}$	heat source	τ	extra Cauchy stress components
T	temperature	ϕ	screw pitch angle.
T_b	barrel temperature		

temperature profile. Rauwendaal [5] developed an analytical expression for the throughput, i.e. the volumetric flow rate of the material through the extruder, and pressure rise for power-law fluids in single-screw extruders. Karian [6] developed an analytical expression for the mechanical power consumption for two-dimensional flow of non-Newtonian fluids in single-screw extruders.

Mitsoulis *et al.* [7] presented a two-dimensional finite element analysis of non-isothermal flow through dies and extruder channels for purely viscous and viscoelastic materials. Elbirli and Lindt [8] proposed a solution for the problem of thermally developing flow in a single-screw extruder where appreciable back flow exists due to the pressure gradient. Later, Lindt [9] discussed the fully developed flow of temperature dependent power-law fluid between parallel plates. An exact solution was developed for this flow in the absence of pressure gradients. Lindt [10] has presented a critical review on the work done by researchers in modeling the melting of polymers in a single-screw extruder. Tadmor and Gogos [1] and Fenner [11] have solved the flow of a polymer in the feed, compression and metering sections of an extruder. Fenner [12] also solved the case of the temperature profile developing along the length of the screw channel. Agur and Vlachopoulos [13] have studied the flow of polymeric materials, which included a model for the flow of solids in the feed hopper, a model for the solid conveying zone and a model for the melt conveying zone. Lawal and Kalyon [14] included wall slip in the numerical simulation.

Gupta *et al.* [15] have developed a three-dimensional finite element model for incompressible flows of non-Newtonian fluids which can be applied to the simulation of single-screw extruders under isothermal conditions. Karwe and Jaluria [16] and Sastrohartono *et al.* [17] have developed two-dimensional models for the simulation of transport processes in single as well as twin-screw extruders, for non-Newtonian fluids. Esseghir and Sernas [18] have carried out an extensive experimental work on the single-screw extrusion process using a fully instrumented single-screw extruder apparatus. Detailed measurements of the temperature profile across the extruder channel were carried out using a cam driven traversing thermocouple. Some results obtained from this work are used to validate the present finite element model, as discussed later.

It is seen that even though the basic transport in the extruder channel is three-dimensional (3D), not much work has been done on simulating the 3D flow. Also, detailed experimental measurements of the temperature field are needed for validation of numerical models. In this paper, the 3D single-screw extrusion process is simulated using the moving barrel formulation. This method of formulation has been adopted by many investigators referred to earlier. In this case, the screw is mathematically treated as unwound and being held stationary with a Cartesian coordinate system attached to it, while the barrel is moved in a direction opposite to the actual screw motion. Using this method, the flow is much easier to visualize and simulate, while the resulting flow behavior would be the same as the actual flow. The finite element method has been used in the simulation. A marching strategy is used to simplify the 3D calculations and the addition

of property variations and chemical reactions in the process. The numerical results obtained are compared with those from the experimental study, indicating fairly good agreement between the two.

2. ANALYSIS AND NUMERICAL SCHEME

In the present work, the flow inside the single-screw extruder is assumed to be a steady-state creeping flow of an incompressible generalized Newtonian fluid. The unwound screw channel, shown in Fig. 1(a), becomes a straight channel with the barrel approximated as an infinite plane. The screw is held stationary, while the barrel is moved above the screw channel in a direction opposite to that of the screw rotation and along the helix angle ϕ of the screw. The velocity components of the barrel are shown in Fig. 1(a) together with the coordinate system. This method of formulation has been adopted by many investigators, see for example Griffith [3], Fenner [12], Elbirli and Lindt [8], Agur and Vlachopoulos [13] and Karwe and Jaluria [16]. Figure 1(b) shows a sketch of the experimental system employed here. The various components of this facility are discussed later.

Furthermore, it is reasonable to assume that the velocity field does not vary significantly along the channel direction, i.e. the z direction. In other words, the derivatives of the velocity components with respect to z are much smaller than those with respect to x or y coordinates and may be neglected. In this case, with the coordinate system chosen above, the velocity field may be represented as:

$$\mathbf{V} = u(x,y)\mathbf{i} + v(x,y)\mathbf{j} + w(x,y)\mathbf{k}. \tag{1}$$

The z component serves as a parameter and brings in the variation along this direction, as seen later. It has been shown, by comparing the results obtained here with those obtained from the full three-dimensional solution by Gupta *et al.* [15], that these approximations are applicable for a wide range of typical operating conditions and that the inclusion of velocity gradients in the z direction does not significantly affect the results.

By neglecting the body force terms, the governing equations are then represented as:

$$\frac{\partial p}{\partial x} = \frac{\partial \tau_{xx}}{\partial x} + \frac{\partial \tau_{xy}}{\partial y} \tag{2}$$

$$\frac{\partial p}{\partial y} = \frac{\partial \tau_{xy}}{\partial x} + \frac{\partial \tau_{yy}}{\partial y} \tag{3}$$

$$\frac{\partial p}{\partial z} = \frac{\partial \tau_{xz}}{\partial x} + \frac{\partial \tau_{yz}}{\partial y} \tag{4}$$

$$\frac{\partial u}{\partial x} + \frac{\partial v}{\partial y} = 0 \tag{5}$$

where the pressure gradient in equation (4) is prescribed to obtain the given flow rate and is thus distinguished from the pressure in the equations (2) and (3), see ref. [19]. The stress components can be represented as:

$$\tau_{xx} = 2\mu\frac{\partial u}{\partial x} \quad \tau_{xy} = \mu\left(\frac{\partial u}{\partial y} + \frac{\partial v}{\partial x}\right)$$

$$\tau_{yy} = 2\mu\frac{\partial v}{\partial y} \quad \tau_{xz} = \mu\frac{\partial w}{\partial x} \quad \tau_{yz} = \mu\frac{\partial w}{\partial y}. \tag{6}$$

The local shear rate, which is the invariant of the rate of deformation tensor, can then be written as:

$$\dot{\gamma} = \left[2\left(\frac{\partial u}{\partial x}\right)^2 + \left(\frac{\partial u}{\partial y} + \frac{\partial v}{\partial x}\right)^2 + 2\left(\frac{\partial v}{\partial y}\right)^2 + \left(\frac{\partial w}{\partial x}\right)^2 + \left(\frac{\partial w}{\partial y}\right)^2\right]^{1/2}. \tag{7}$$

In the present study, several viscosity models, representing the shear rate and temperature dependence of the materials, are used and will be given during the discussion of the results obtained.

The flow in the screw channel is solved in terms of the cross-channel and down-channel flows. The cross-channel flow is defined by u and v velocity components on the x–y plane and represented by equations (2), (3) and (5), while the down-channel flow is defined by w velocity component in the z-direction and governed by equation (4). The cross- and down-channel flow are coupled through equations (6)–(7) for a non-Newtonian case, but in the Newtonian case, they are independent of each other.

The corresponding energy equation for the given flow situation is:

$$\rho C_p\left(u\frac{\partial T}{\partial x} + v\frac{\partial T}{\partial y} + w\frac{\partial T}{\partial z}\right) = \frac{\partial}{\partial x}\left(k\frac{\partial T}{\partial x}\right) + \frac{\partial}{\partial y}\left(k\frac{\partial T}{\partial y}\right) + \dot{Q}. \tag{8}$$

Here, convection terms are retained since the fluids considered have a very high Prandtl number, Pr. $\dot{Q}$ is the heat source due to viscous dissipation and is given as:

$$\dot{Q} = \mu\dot{\gamma}^2. \tag{9}$$

The above equations govern the thermomechanical process of extrusion. All these assumptions were validated by comparisons with results from a full, elliptic, 3D numerical formulation [15]. It was shown by Sastrohartono [19] that the present simplified model yields accurate results for the problem under consideration with much smaller CPU time and much smaller computer storage requirements.

The finite element method for solving the x and y momentum equations, together with the continuity equation, was formulated on the basis of the principle of virtual velocity [20]. Details of the scheme are given by Sastrohartono [19]. In the present study, a quadratic six-node triangular element has been used, where three nodal points are located at the vertices and the

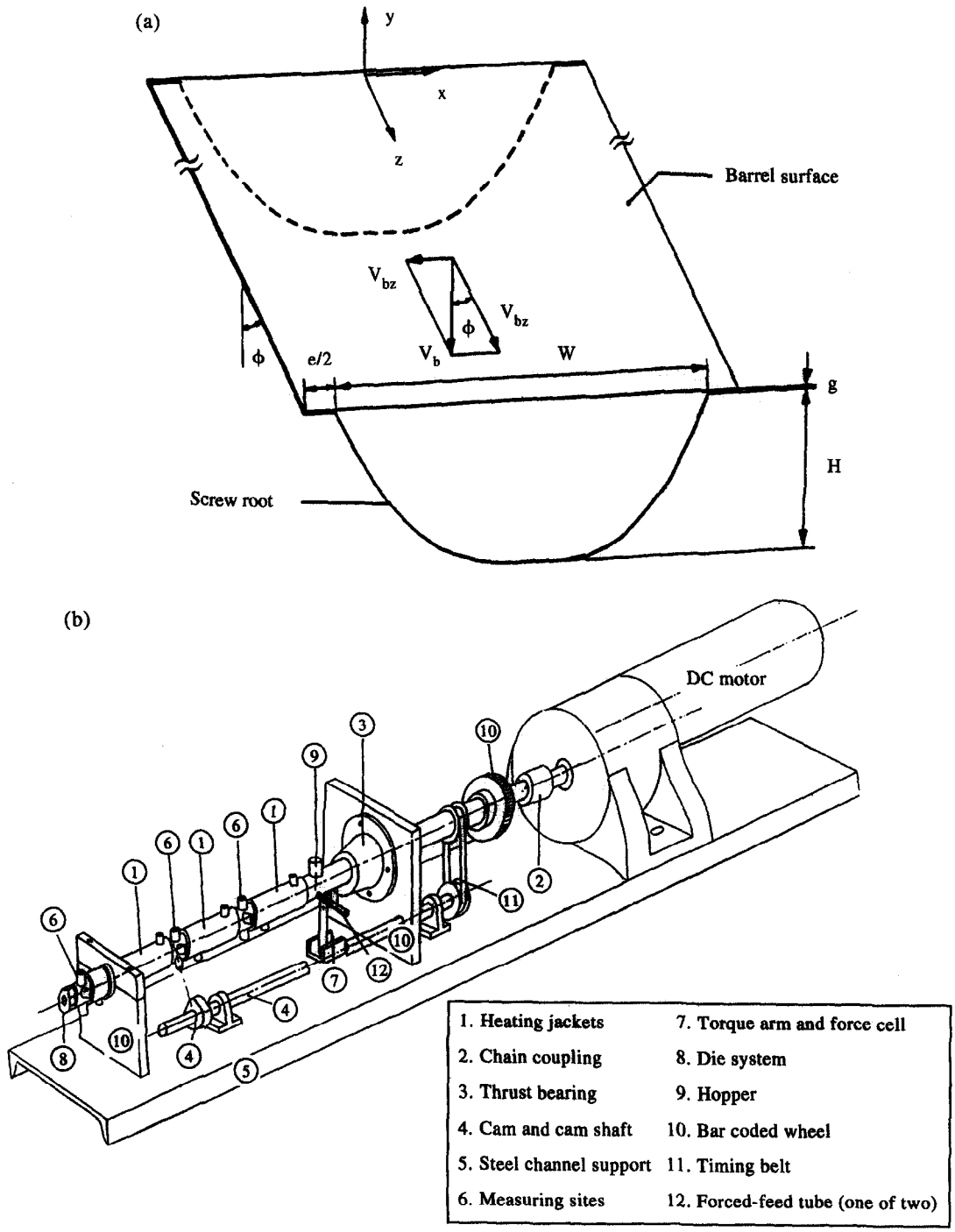

Fig. 1. (a) Unwound screw channel with the coordinate system for the moving-barrel formulation. (b) Schematic view of the single-screw experimental facility.

other three nodal points are at the middle of the sides. The velocity and pressure are approximated within an element in terms of the velocity and pressure nodal point values. Quadratic and linear approximations for the velocity and pressure points, respectively, have been used.

The finite element formulation for the z-momentum equation is obtained by using the Galerkin method, where the weighting functions are the shape functions for the velocity field [21]. The Galerkin method is based on the method of weighted residuals, a method which can be used to obtain approximate solutions to linear and nonlinear differential equations. In this method, the exact solution is approximated by a function, and the weighted residuals, i.e. the integral over the domain of the error multiplied by the weighting

functions, must vanish. Further details on this method are given in, for example, refs. [22–24]. The finite element formulation for the energy equation is also based on the Galerkin method, where the weighting functions are the shape functions for the temperature field.

The heat transfer process is governed by the energy equation which is parabolic in the z direction. Therefore, a marching scheme in the down-channel (z) direction, with an iteration process being employed at every z location, is needed for solving these non-linear equations. The advantage of such a marching scheme, as compared to the solution of the full 3D, elliptic, problem lies in much smaller CPU times and much less computer storage needed. It is also much easier to incorporate property changes and chemical reaction effects in this scheme. In fact, the ease with which changes in the material characteristics can be included in the scheme for a marching procedure was the main reason for using this approach.

3. NUMERICAL RESULTS AND DISCUSSION

The computational domain is represented by the screw channel, with its cross-section as the desired screw profile. The three-dimensional flow is modeled by marching in the down channel direction, as represented by the parabolic nature of the energy equation in the z or down channel direction. The numerical computation is carried out on a slice by slice basis, in which the cross-section of the screw channel is used for solving the energy and momentum equations and a marching scheme for the down channel direction. Therefore, the model is not a fully three-dimensional elliptic one, but may be termed as quasi-three-dimensional. For the sake of brevity, however, the current FEM model will be referred to as a three-dimensional model. The mass conservation in the x and y plane is assured by the continuity equation, equation (5), while mass conservation in the z direction is obtained through the prescribed mass flow rate. The marching term is contained in the energy equation. Therefore, the energy equation is solved first at every new cross-section after marching, followed by the momentum equations.

3.1. *Fluids considered*

Three different fluids are employed in the numerical simulation. These are low-density polyethylene (LDPE), viscasil 300-M and heavy corn syrup. The viscosity model of LDPE is given as [1]:

$$\mu = \mu_0 \left(\frac{\dot{\gamma}}{\dot{\gamma}_0}\right)^{n-1} \exp\left[-b(T-T_0)\right] \qquad (10)$$

where μ is the viscosity in Pa s, $\mu_0 = 2000$ Pa s is the reference viscosity at 200°C, $\dot{\gamma}$ is the shear rate, $\dot{\gamma}_0 = 1$ s^{-1} is the reference shear rate, $n = 0.48$ is the power-law index, $b = 0.01\,^{\circ}C^{-1}$ is the temperature coefficient, T is temperature in °C and T_0 is the reference temperature, taken as 200°C. Other properties of LDPE are: $\rho = 750$ kg m^{-3}, $k = 0.30$ W m^{-1} K^{-1} and $C_p = 2500$ J kg^{-1} K^{-1} [11].

Like LDPE, Viscasil is also a non-Newtonian fluid. The viscosity model for Viscasil 300-M is given as [25]:

$$\mu = \frac{A\exp\left(\frac{B}{T}\right)}{1+C\left[A\exp\left(\frac{B}{T}\right)\dot{\gamma}\right]^{1-n}} \qquad (11)$$

where μ is viscosity in poise, T is temperature in K, and $\dot{\gamma}$ is shear rate in s^{-1}. The values of the constants are: $A = 0.7249023$ poise, $B = 2560.804$ K, $C = 7.42082 \times 10^5$(N m^{-2})$^{n-1}$, power-law index $n = 0.2671$, and density $\rho = 979$ kg m^{-3}. The thermal conductivity and the specific heat are: $k = 0.155758$ W m^{-1} K^{-1}, $C_p = 1507.16$ J kg^{-1} K^{-1}. Both equations (10) and (11) are valid over the range of temperatures and shear rates considered here, these being for typical extruder operating conditions.

In contrast to the previous fluids, corn syrup is a Newtonian fluid. The viscosity model for corn syrup is given as [25]:

$$\mu = 1052.58\exp\left[-0.095(T-20)\right] \qquad (12)$$

where μ is in poise and T is in °C. The thermal properties for corn syrup are: $k = 0.317$ W m^{-1} K^{-1}, $C_p = 2015$ J kg^{-1} K^{-1}, and the density $\rho = 1381$ kg m^{-3}.

3.2. *Flow and heat transfer*

A study of the flow and heat transfer was carried out for a single-screw extruder with the commonly used self-wiping profile of Werner–Pfleiderer ZSK-30 screw element shown in Fig. 1(a). The velocity and temperature fields were studied in detail for various operating conditions. The profile of the self-wiping screw channel was obtained from the expression derived by Booy [26, 27] and by Hwang [28]. This screw element has the following dimensions: pitch $t = 28.0$ mm, helix angle $\phi = 16.1888°$, maximum channel depth $H = 4.7$ mm, maximum channel width $W = 11.52$ mm, screw tip width $e = 1.924$ mm, and gap between screw tip and barrel $g = 0.075$ mm.

The same screw elements were used in constructing a single-screw experimental apparatus devised by Esseghir [25] for his experimental work [see Fig. 1(b)]. Later, some of the results of this experimental work will be used for validation of the present FEM model. The results presented here are for a single-screw extruder having exactly the same dimensions as the experimental apparatus. The single-screw experimental apparatus had three sections of water jacket which are used for cooling or heating the barrel and can be adjusted individually to maintain a desired water temperature level. The notation $T_{b1}/T_{b2}/T_{b3}$ is used throughout the discussion to represent a combination of barrel temperatures T_{b1}, T_{b2} and T_{b3} at

sections 1, 2 and 3 of the water jacket, respectively. The lengths of the water jackets are 120, 90 and 120 mm, respectively, giving a total length of the single-screw extruder apparatus of 330 mm. This axial length corresponds to a 1180 mm long unwound screw channel used in the simulation.

The thermal boundary conditions at the screw surface may be taken as isothermal. However, a more practical circumstance is represented by the adiabatic condition at the screw surface, which is employed in the present study. A more accurate approach is to take into account the conduction within the screw and the barrel, in which case a conjugate heat transfer problem must be solved. The thermal boundary condition at the barrel surface is taken as a prescribed temperature.

3.3. *Heat input at the barrel*

For the first circumstance presented here, the barrel is set at a temperature higher than the inlet temperature. For a given extruder design and working fluid, the input parameters for the program are: screw rotational speed (RPM), inlet temperature, barrel temperature distribution along the extruder and the desired volumetric flow rate. The flow and temperature field along the extruder can be plotted from the results of the simulation as the longitudinal flow and temperature distribution along the mid-width of the channel. We can also study the flow and temperature field over the cross-section at any down channel position. The dimensionless parameters used in the following figures are defined as follows:

$$z^* = z/H \quad y^* = y/H \tag{13}$$

$$T^* = (T-T_i)/(T_b-T_i) \quad \text{and} \quad w^* = w/V_{bz}.$$

The volumetric flow rate can be non-dimensionalized as:

$$q_v = \frac{\text{Volume flow rate}}{(\text{Screw area})\,V_{bz}} \tag{14}$$

where the screw area is WH for a rectangular profile.

Figures 2 and 3 show the results of the simulation for the case when the three portions of the barrel are set at temperatures $T_b = 40, 60, 80°C$, over the length of 120, 90 and 120 mm, respectively. The highest temperature at the barrel is used to define the dimensionless temperature T^*. The screw speed is 60 rpm, the inlet temperature $T_i = 24°C$, and the normalized flow rate $q_v = 0.32$. Figure 2 shows the development of the flow and the temperature along the down channel direction. The temperature and w velocity contours are shown at the midplane of the channel while the corresponding profiles are shown at four locations along the channel. The first location represents the inlet, or hopper, of the extruder for this fluid, while the last location corresponds to the die. The second and third locations are situated between the first and second water jackets and between the second and third water jackets, respectively, of the single-screw extruder apparatus. At the second and third locations, sudden changes in the barrel temperature take place. The effect of the barrel temperatures on the temperature and w velocity fields are shown in this figure by the disturbed temperature and w velocity contours and changes in their profiles. Due to the heat input at the barrel, the fluid temperature rises along the channel. The isotherms show that the fluid at the mid-width of the channel gets hotter as it flows towards the die due to heat transfer and viscous dissipation. The local viscosity of the fluid decreases as the local temperature rises. The viscosity changes result in changes in the w velocity field since the flow rate, or throughput, is maintained constant in the extruder for steady state conditions.

The flow and temperature fields across the channel cross-section are shown in Fig. 3 at a downstream location. The velocity profile shows a counter clockwise recirculating flow across the screw channel, which, together with the down channel velocity component, results in a spiral motion of the material along the channel. The center of this recirculation flow is located about 1/3 of the screw channel depth from the moving barrel, which is in agreement with the analytical solution. The effect of the recirculating flow is seen in the temperature profile as the heating up of the fluid near the screw root. The pressure contours show a more uniform pressure level across the channel as the fluid flows farther downstream.

As the material flows, it rises in temperature due to the heat input from the barrel and from viscous dissipation. Thus it becomes less and less viscous. The resulting down channel pressure gradient, therefore, decreases downstream, since the flow rate is constant. The corresponding pressure, pressure gradient, the bulk temperature and the heat transfer characteristics along the screw channel are shown in Fig. 4. It is seen that the pressure gradient decreases monotonically along the channel except at the points where a sudden change in temperature takes place. Of course, in actual practice the change in temperature will be more gradual and this effect is not expected to arise. The bulk temperature rise along the channel also shows the effect of the application of different barrel temperatures. It is seen that the bulk temperature rises quickly to reach the barrel temperature level. It was found that the recirculation flow in the screw channel promotes a faster temperature rise in the fluid due to the heating from the barrel and thus enhances uniformity of the fluid temperature across the cross-section.

During extruder operation, the direction of the heat transfer process depends on the temperature difference between the barrel and the fluid. In the present study, the heat flux from/to the barrel is defined as:

$$q(x,z) = k(\mathrm{d}T/\mathrm{d}y)|_{\text{barrel}} \tag{15}$$

where $q(x,z)$ is the local heat flux as a function of the x and z locations, and $\mathrm{d}T/\mathrm{d}y|_{\text{barrel}}$ is the temperature gradient evaluated in the fluid at the barrel surface. A positive heat flux implies heat is being transferred

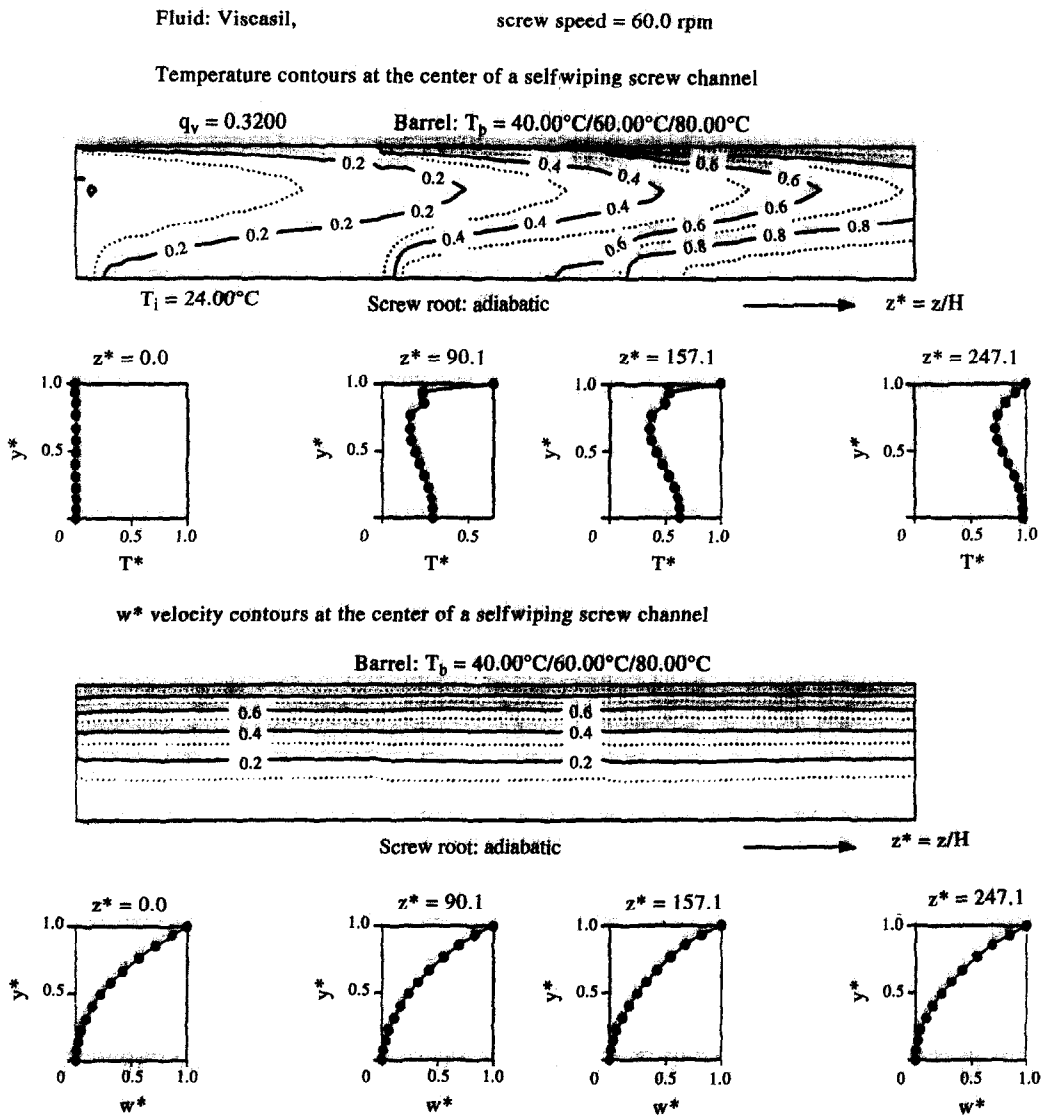

Fig. 2. Flow and temperature fields along the screw channel of a single screw extruder with a ZSK-30 self-wiping screw profile. Fluid: Viscasil-300M, T_i = 24°C, T_b = 40/60/80°C, q_v = 0.32, N = 60 rpm.

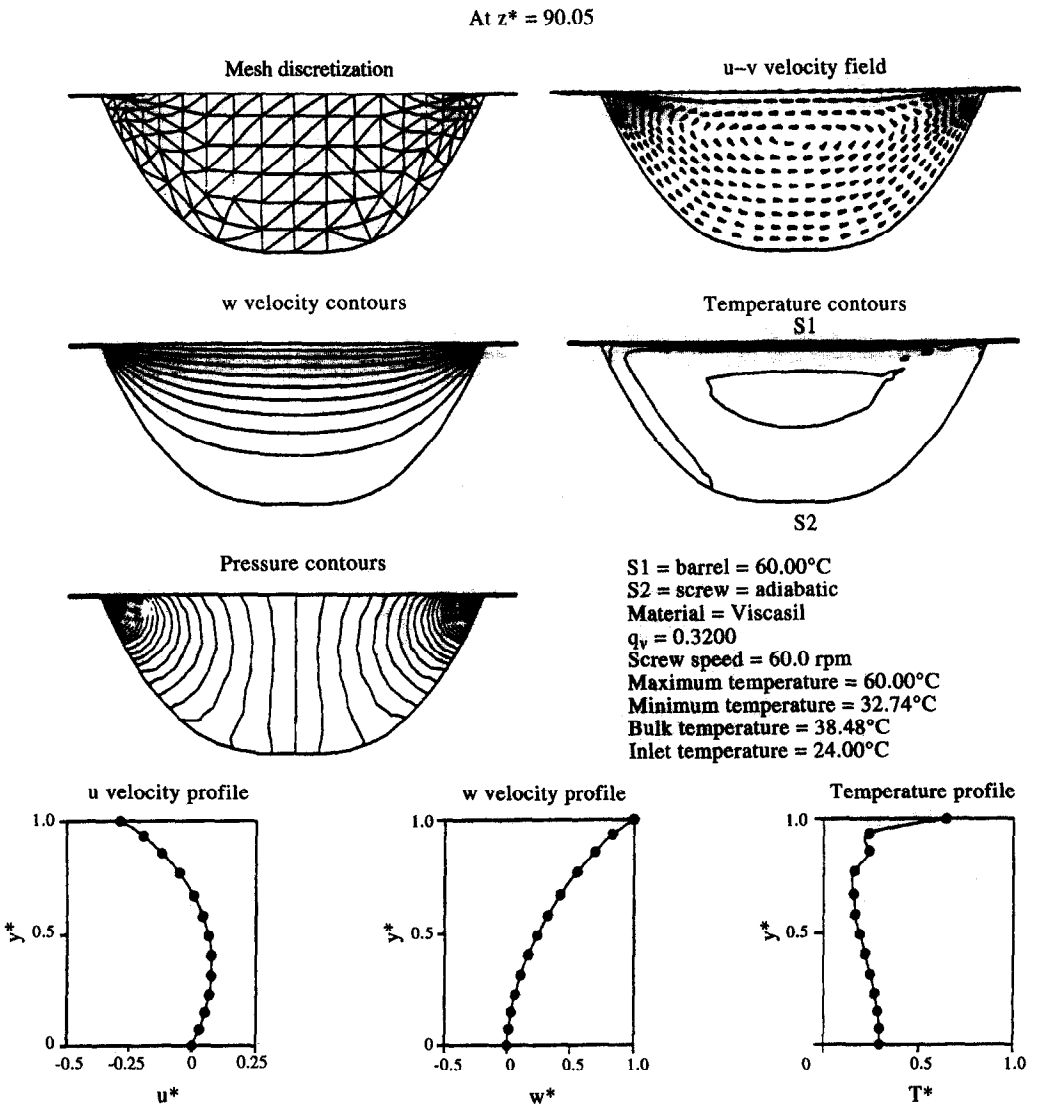

Fig. 3. Cross-sectional flow and temperature field at $z^* = 90.05$. Fluid: Viscasil-300M, $T_i = 24°C$, $T_b = 40/60/80°C$, $q_v = 0.32$, $N = 60$ rpm.

from the barrel to the fluid, while a negative value means heat is being transferred from the fluid to the barrel. The channel-width-averaged local heat flux $q(z)$ is calculated as:

$$q(z) = \frac{1}{W}\int_{-W/2}^{W/2} q(x, z)\,dx \tag{16}$$

where W is the channel width. The local heat transfer coefficient $h(z)$ and the Nusselt number $Nu_H(z)$ are defined as:

$$h(z) = \frac{q(z)}{T_{b_{ref}} - T_i} \tag{17}$$

$$Nu_H(z) = \frac{h(z)H}{k} \tag{18}$$

where $Nu_H(z)$ is the local Nusselt number based on the screw channel height H, $T_{b_{ref}}$ is the reference barrel temperature, and T_i is the inlet temperature. The overall average heat transfer coefficient for the extruder can be calculated as:

$$\bar{h} = \frac{1}{L}\int_0^L h(z)\,dz \tag{19}$$

where L is the screw channel length. Similarly, the overall average Nusselt number is given as

$$\overline{Nu}_H = \frac{1}{L}\int_0^L Nu_H(z)\,dz. \tag{20}$$

For the present case, the variation of the heat transfer coefficient h and the Nusselt number along the channel is shown in Fig. 4(c), where $T_{b_{ref}} = 80°C$. Since the fluid temperature is always lower than the barrel temperature, in this case, the heat flux is positive everywhere, representing heat being transferred from

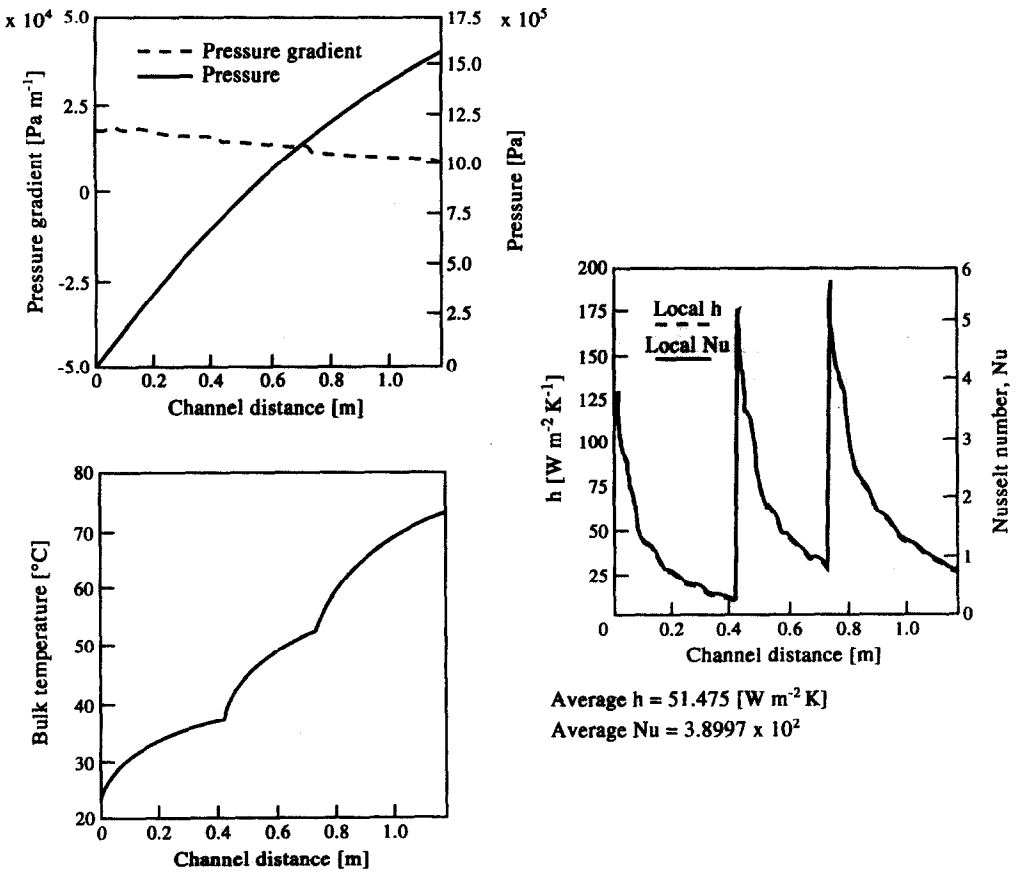

Fig. 4. Variation of pressure, pressure gradient, bulk temperature, heat transfer coefficient h and Nusselt number Nu_H at the barrel along the screw channel. Fluid: Viscasil-300M, $T_i = 24°C$, $T_b = 40/60/80°C$, $q_v = 0.32$, $N = 60$ rpm.

the barrel to the fluid. The jumps in the curve occur at the positions where step changes in the barrel temperature take place.

The shear rate in the flow is shown in Fig. 5. The shear rate contours along the channel show the effect of the barrel temperatures on the flow. The shear rate contours across the channel are symmetric about the mid-plane of the channel, as expected. The maximum shear rate arises in the gap between the screw tip and the barrel where there is a large velocity difference between the moving barrel and the stationary screw within a small gap, while the minimum is found at the screw root where the velocity gradient is smallest.

Figure 6 shows the flow and temperature fields along the mid-plane of the screw channel in terms of the isotherms, velocity contour lines, and profiles for the temperature and w velocity component. In this simulation, the temperature of the first section of the barrel was kept at the same level as the inlet temperature. The effect of the slightly higher temperature at the second and third sections of the barrel on the fluid temperature is clearly seen in the temperature contours along the center of the channel. The changes in the w velocity field are also seen in the w^* contours at a downstream location, located about one third of the screw length from the inlet, at the interface between the first and the second water jackets.

Similar trends, as seen in the previous results, are observed in the current case. The variation of the pressure, bulk temperature, and heat transfer coefficient of the fluid along the channel are shown in Fig. 7. The pressure is seen to increase linearly along the screw channel with a change in the gradient evident at the location where the barrel temperature is increased. Since the temperature of the first section of the barrel was set at the same level as the inlet temperature, the increase of the bulk temperature of the fluid in this section above the inlet temperature is due to the viscous dissipation. It is also seen in the plot that the temperature across the channel cross-section is uniform over much of the channel length and that the bulk temperature of the fluid increases from about 25°C to about 40°C over a distance of about 30 mm. It was found that, as the screw rotational speed (rpm) is increased, the effect of heating from the barrel on the fluid temperature is smaller, since the fluid spends less time in the extruder. It was also found that, in general, the viscous dissipation effect is relatively small for small speeds, as expected.

It was found that some heat is transferred from the

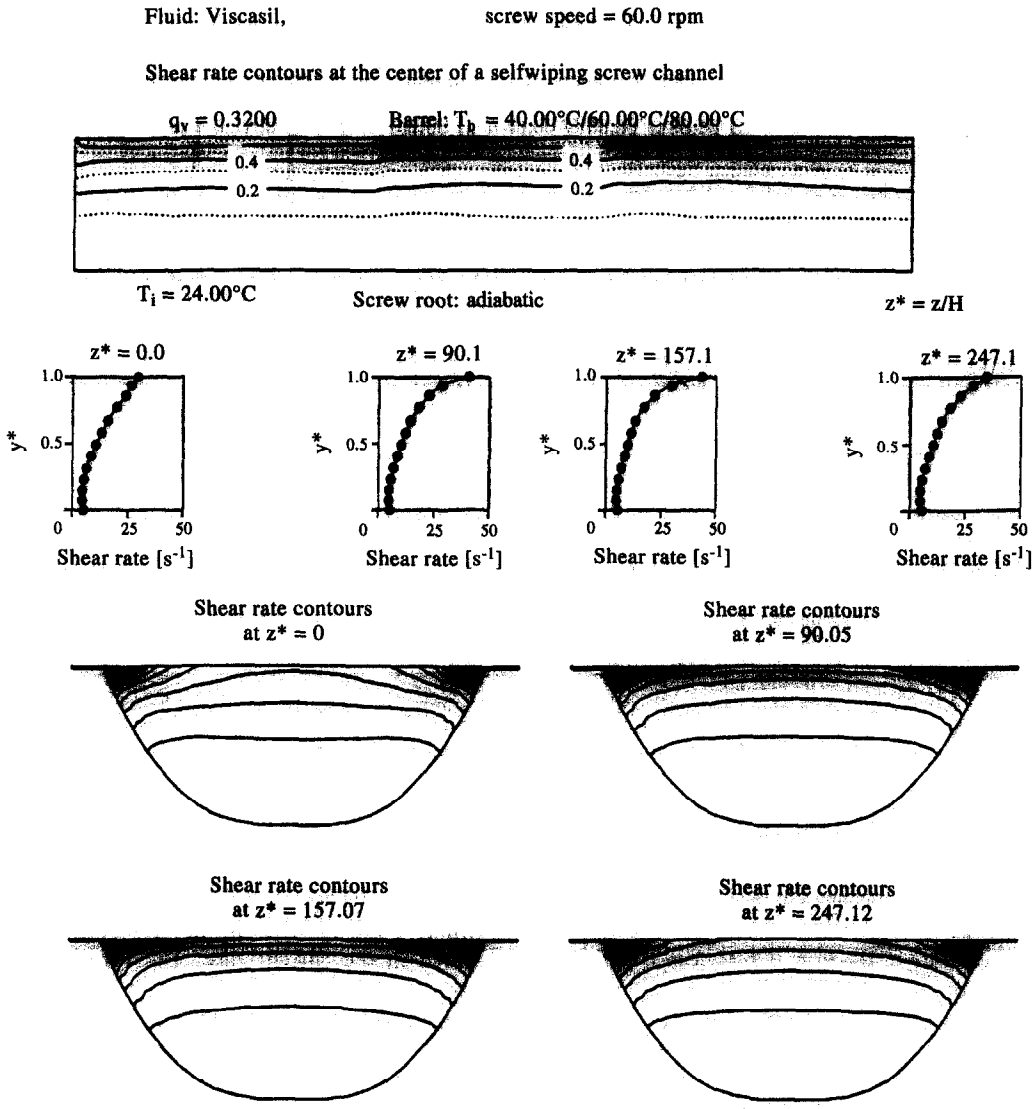

Fig. 5. Shear rate contours along the channel and shear rate profiles across the channel at four down channel locations. Fluid : Viscasil-300M, T_i = 24°C, T_b = 40/60/80°C, q_v = 0.32, N = 60 rpm.

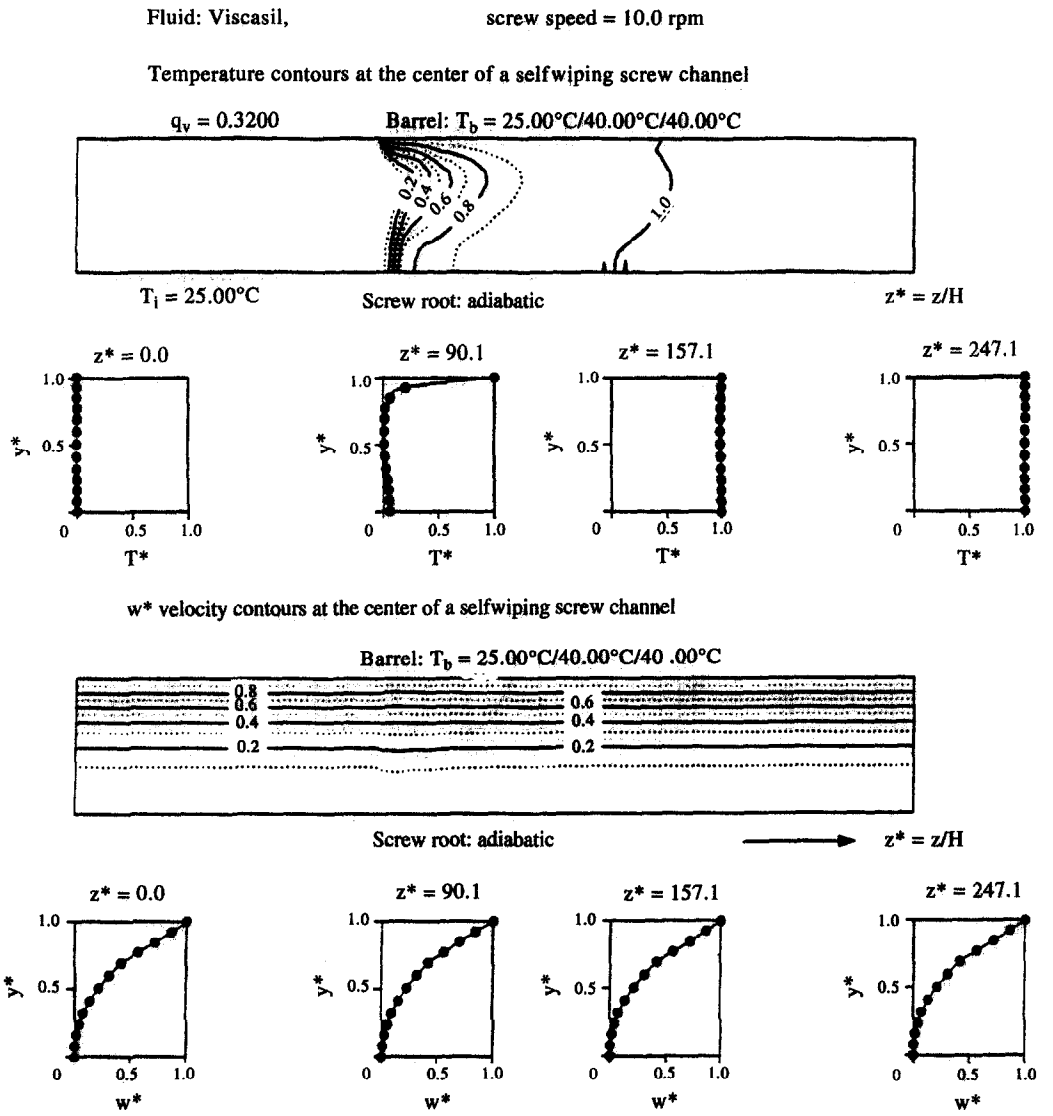

Fig. 6. Flow and temperature fields along the screw channel of a single screw extruder with a ZSK-30 self-wiping screw profile. Fluid: Viscasil-300M, T_i = 25°C, T_b = 25/40/40°C, q_v = 0.32, N = 10 rpm.

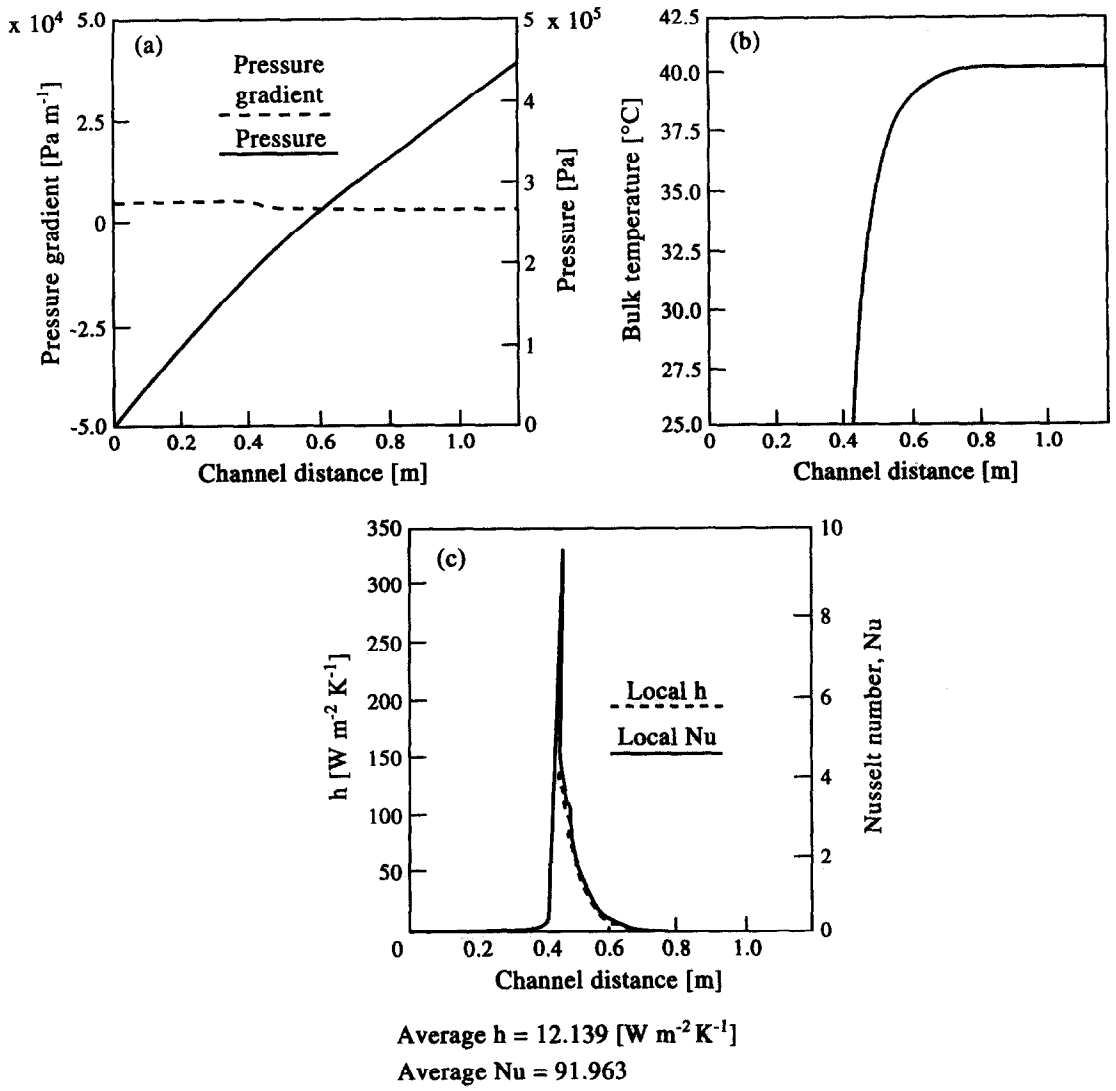

Fig. 7. Variation of (a) pressure, (b) bulk temperature, and (c) heat transfer coefficient along the screw channel. Fluid : Viscasil-300M, $T_i = 25°C$, $T_b = 25/40/40°C$, $q_v = 0.32$, $N = 10$ rpm.

fluid to the barrel along the first barrel section. The increase in fluid temperature above the barrel temperature is due to the viscous dissipation. In the second barrel section, however, where the barrel temperature is set at a higher temperature, heat is transferred from the barrel to the fluid. Finally, due to the viscous dissipation effect, the fluid temperature becomes higher than the barrel temperature so that some heat is transferred from the fluid to the barrel in the last portion of the barrel. The heat transfer coefficient was calculated using a reference barrel temperature $T_{b_{ref}} = 40°C$. Similar trends were observed at other speed and barrel temperature settings.

3.4. *Effect of flow rate*

The effect of flow rate on the pressure and temperature at the die for a given screw rotational speed was investigated. Figure 8 shows the variation of the die pressure and temperature with the normalized flow rate q_v for three different screw speeds, with the barrel at a uniform temperature $T_b = 80°C$, inlet temperature $T_i = 24°C$ and Viscasil as the working fluid. As can be seen in this figure, the die pressure decreases as the flow rate increases for a given screw speed. The pressure eventually becomes negative as the flow rate increases, since the extruder cannot pump out the required flow rate by itself. In other words, the material needs to be pressurized at the hopper in order for the extruder to deliver the required flow rate. The condition when the die pressure is zero corresponds to the no-die situation. The common operating range of the extruder in practice is the one which produces a positive die pressure. It can also be seen that, for a given q_v, the pressure difference between the hopper and the die is larger when the screw speed is higher, due to the higher flow rate. It is also shown that for the no-die situation, one can pump more fluid by increasing the screw speed.

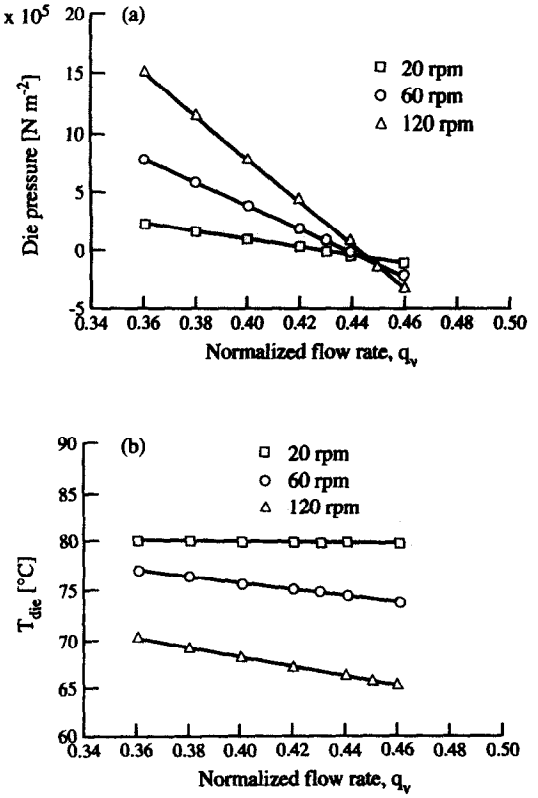

Fig. 8. Variation of the (a) die pressure (b) die temperature with the normalized flow rate q_v for different screw speeds.

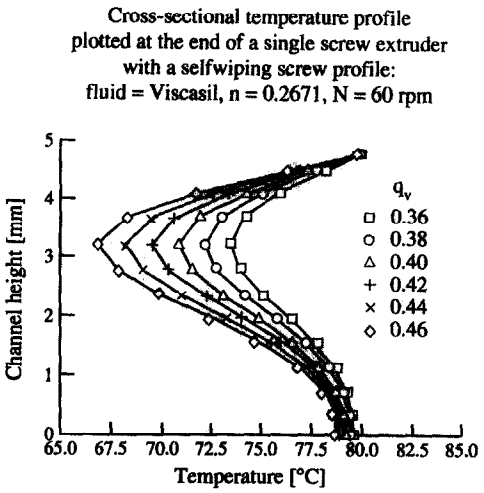

Fig. 9. Temperature profile at the mid-plane of the channel, as affected by the flow rate, at a constant screw speed of 60 rpm.

It is seen that the die temperature is higher for a lower flow rate at a given screw speed. Keeping the normalized flow rate q_v the same, a higher screw speed results in a lower die temperature, since the higher flow rate causes the material to stay for a shorter time in the extruder, thus obtaining less heat from the barrel. The same reasons explain a lower temperature at a higher flow rate, for a given screw speed.

The effect of flow rate on the temperature profile at the center of the channel is shown in Fig. 9 at the end of the screw channel, for a constant screw speed of 60 RPM and the same barrel and inlet temperatures as before. As discussed earlier, the temperature profile is affected by the recirculating flow in the channel. As the flow rate increases, the fluid flow becomes faster in the channel and, thus, decreases the residence time of the fluid inside the channel. This shortens the heat transfer process between the hotter and cooler fluid. Thus, the shorter residence time results in more inhomogeneity of the temperature across the channel. As shown in this figure for the case of heating from the barrel, the fluid in the inner part of the channel has a lower temperature than the fluid in the outer part of the channel.

3.5. *Experimental results and comparisons*

The experimental results presented here were obtained by Esseghir and Sernas [18] and Sabol [29], using a single-screw apparatus which is constructed using the self-wiping screw profile described earlier. The characteristics of a single-screw extruder operation can be presented as a set of pressure vs flow rate curves for a given material at various operating temperatures. The characteristic curves are also called the pumping characteristics of a single screw extruder since the curves show the variation of pressure at the die with the throughput. For a given single-screw extruder, die, material and operating temperature, the throughput can be varied by changing screw speed. A higher throughput will obviously result in a higher die pressure. The characteristic curves are therefore very important, since they can be used as a guide for operating the extruder.

In validating the FEM model, the FEM predictions of the pumping characteristics of the single-screw extruder apparatus are compared to the experimental results obtained by Esseghir [25], using Newtonian as well as non-Newtonian fluids. Using corn syrup as the working fluid, the comparisons are shown in Fig. 10(a) for isothermal conditions at 30 and 35°C, respectively, using a 2.0 mm die. It can be seen from this figure that the FEM predictions give a very good agreement with the experimental results. The good agreement can be attributed in part to the exact profile and dimensions of the screw channel being used in the FEM model and establishes the validity of the numerical model. A similar comparison was obtained for an isothermal condition at 30°C and a 3.6 mm die.

The comparison of the results of numerical and experimental studies using a non-Newtonian fluid for isothermal flow is presented in Fig. 10(b). In this case, the FEM model assumed an isothermal, fully developed flow in the down channel direction. The fluid and the barrel temperatures were taken as 80°C. A rectangular screw profile with dimensions W and H_{max} was also used in the simulation to show the

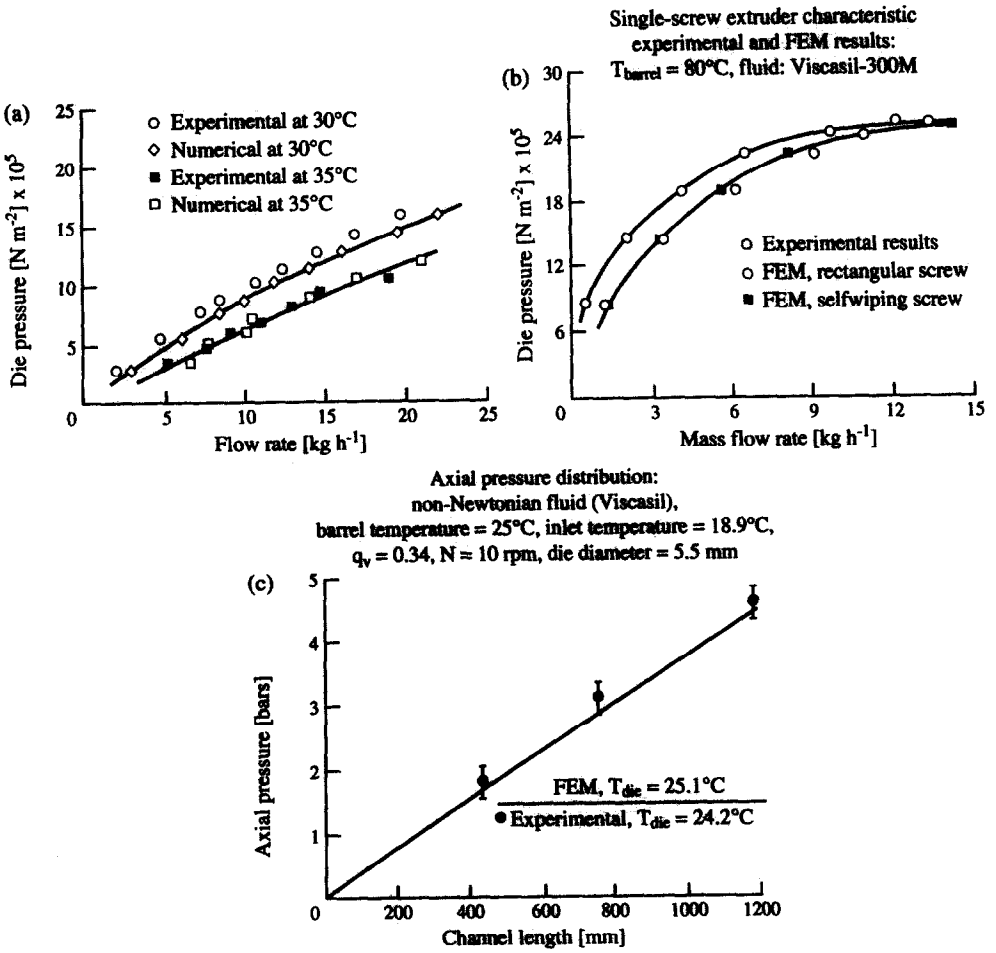

Fig. 10. (a) Comparison between 3D (FEM) predictions and experimental results of Esseghir [25] for the single-screw extruder. Fluid = corn syrup, isothermal at 30 and 35°C, 2.0 mm die. (b) Fluid = Viscasil, isothermal at 80°C, 2.4 mm die. (c) Fluid = Viscasil, N = 10 rpm, T_b = 25.0°C, T_i = 18.9°C, 5.5 mm die.

magnitude of the error one would get from using a rectangular approximation to the actual screw profile. It can also be seen from this figure that a good agreement between the numerical and experimental results arises when the real screw profile is used in the simulation. The higher die pressure for the rectangular screw profile than that for the self-wiping screw profile, at a given flow rate, is due to the larger cross-sectional area of the rectangular screw profile.

Further verification of the present FEM model with the experimental results was carried out in terms of the pressure distribution along a nonisothermal screw channel with Viscasil as a non-Newtonian working fluid. Figure 10(c) shows the comparison of the finite element model with the experimental results obtained by Sabol [29, 30] for barrel temperatures of 25/25/25°C, die diameter of 5.5 mm, and screw speed of 10 rpm. At this speed, the screw is completely filled. This figure shows that the FEM predictions are in a good agreement with the experimental results. It might be mentioned here that the uncertainty in the pressure measurements was ±0.30 bars [29–30]. It was found and discussed in ref. [31] that there is a temperature difference which exists between the water jacket and the inner barrel wall. This difference, although not accurately known, is not negligible. Since the present FEM model does not consider the conjugate problem, the prescribed barrel temperature used in the model should be the temperature of the inner surface of the barrel, which is not measured here, rather than the water temperature which is measured.

The temperature profiles at the mid-plane of the channel as computed by the 3D (FEM) model and measured by the experimental work for Case I (Table 1) are shown in Fig. 11(a), while 11(b) shows the comparison between the 2D (FDM) predictions [16] and experimental results. For this experiment, the barrel temperature distribution was 11.9/8/8°C, inlet was at 22.0°C and N = 20 rpm. As can be seen, the 3D model predicts the temperature to within 0.5°C accuracy and maintains the shape of the temperature distribution. The 2D model, however, does not obtain the experimentally measured temperature profile as its predicted temperature gradually increases towards the screw root. The two comparisons show the importance of the recirculating flow inside the channel. In

Table 1. Comparison between numerical (3D-FEM and 2D-FDM) and experimental results in terms of T_{Die}, P_{Die} and T_s

Test	Die pressure P_{Die}			Bulk temperature at Die T_{Die}			Temperature at screw root T_s		
	Exp.[1]	FDM[2]	FEM	Exp.[1]	FDM[2]	FEM	Exp.[1]	FDM[2]	FEM
Case I	21.0	18.2	16.4	13.0	13.05	12.4	12.6	16.89	12.6
Case II	20.4	23.1	18.2	12.9	12.77	12.6	12.8	14.25	12.7
Case III	11.34	10.5	7.50	22.0[3]	22.3	22.6	22.2	21.42	22.6

[1] Experimental work [25, 18].
[2] Computed results.
[3] T_{Die} ranged from 21.7 to 22.8°C due to variations in T_{inlet}.

the case of the 3D model prediction, the recirculating flow enhances the heat transfer process within the channel, resulting in cooling of the fluid near the screw root due to the lower barrel temperature. On the other hand, the two-dimensional approximation of the FDM model does not capture this recirculation. The resulting temperature distribution, therefore, shows higher temperature of the fluid near the screw root than the measured one, since the warmer fluid remains located near the screw root and the cooling process takes place only from the fluid to the barrel. It is also interesting to note that the predicted maximum temperature by the 3D (FEM) model is located at 2/3 of the channel height from the screw root. This location corresponds to the center of the recirculation flow for a Newtonian fluid within a rectangular cavity with a moving top plate.

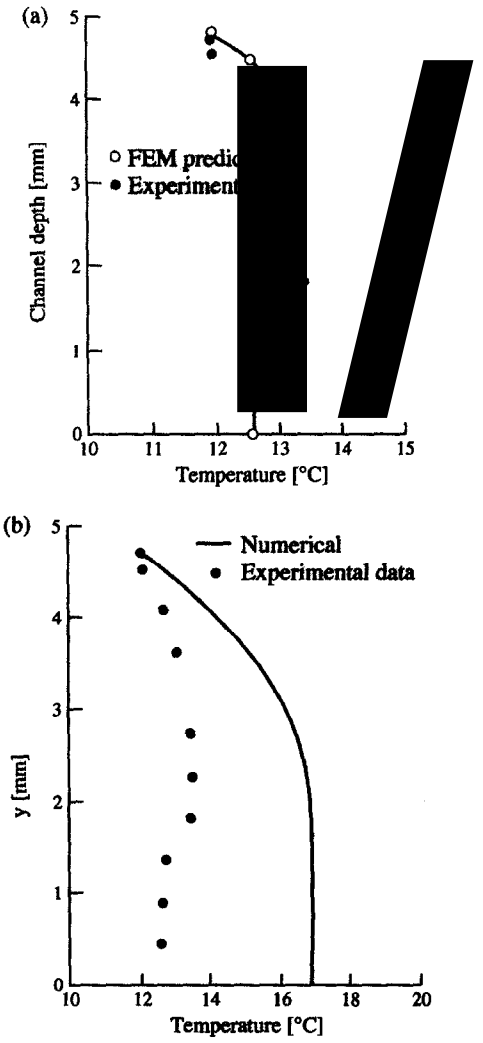

Fig. 11. Comparison between numerically calculated and experimentally measured [25, 18] temperature profiles for Case I. (a) 3D (FEM), and (b) 2D (FDM).

The effect of uniform cooling from the barrel was investigated to see whether or not the fluid temperature would become uniform after traveling a certain distance. Figure 12(a) and (b) shows the comparison between the experimental and numerical results from 3D (FEM) and 2D (FDM), respectively, for Case II (Table 1). For this experiment the barrel temperature distribution was 12.2/12.2/12.2°C, inlet was at 20.3°C and $N = 20$ rpm. As can be seen, the 3D model predicts the correct temperature at the screw root, while the 2D model predicts a higher screw root temperature than the measured one. The experimental data show more or less a uniform temperature distribution, as one would expect, from the uniform cooling due to the barrel. In this case, the 2D model gives a better accuracy than in the previous case. Nevertheless, the 2D results still show an increasing temperature towards the screw root caused by delayed cooling from the barrel. This discrepancy, again, can be attributed to the inability of the 2D model to capture the recirculation flow, since this is a two-dimensional model.

The results for another case, shown in Fig. 12(c) and (d), give the comparison for Case III (Table 1). For this experiment the barrel temperature distribution was 22.3/22.3/22.3°C and $N = 35$ rpm. The experimental data for the temperature profile corresponded to a given inlet temperature distribution. The inlet temperature varied from 18.1–19.25°C, from the bottom point to the top. In this case an average inlet temperature $T_i = 18.8$°C was used in the numerical simulation using the 3D (FEM) model. As expected, the results show that the agreement is better at the upper part of the profile, where the inlet temperatures were around 19°C during the experimental investigation. A better prediction would be obtained if one takes the exact inlet temperature for each data point. Nevertheless, the 3D model still predicts the temperature profile within 0.5°C accuracy. The 2D

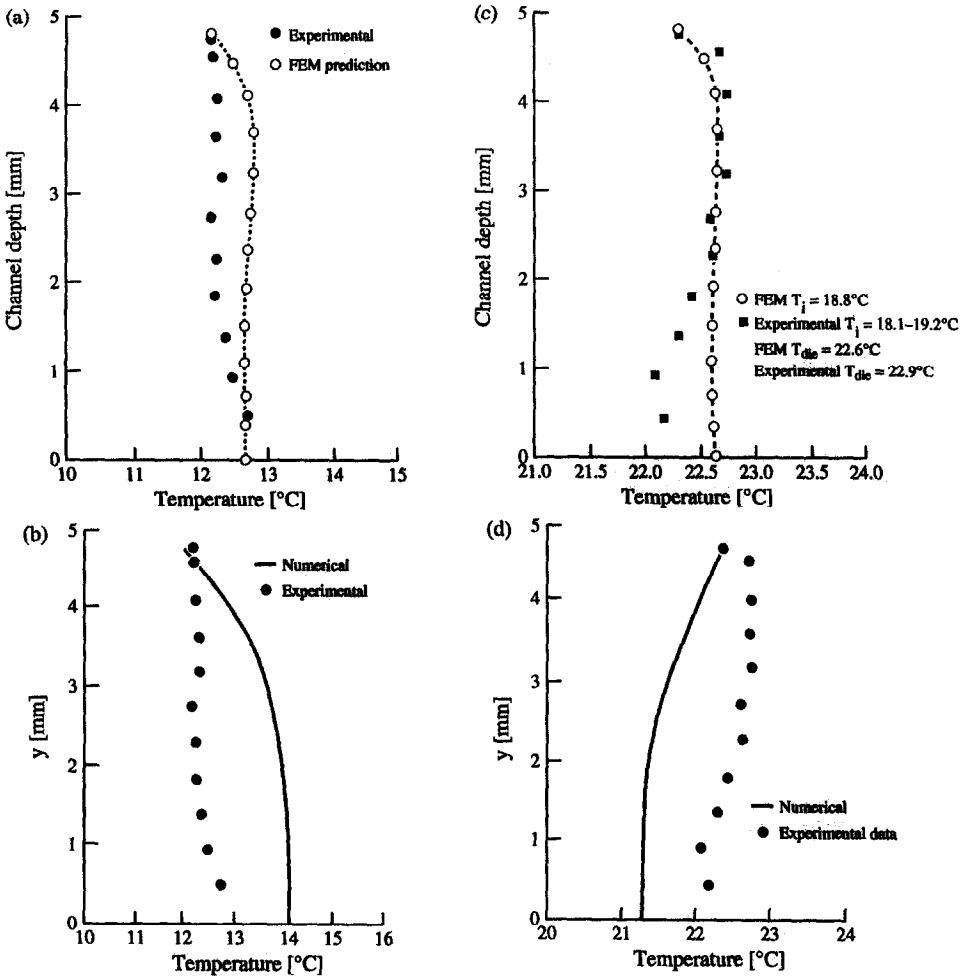

Fig. 12. Comparison between numerically calculated and experimentally measured [25,18] temperature profiles. (a) and (c) 3D (FEM) and (b) and (d) 2D (FDM); (a) and (b) are of Case II and (c) and (d) are of Case III.

model predicts a lower temperature at the screw root than the experimentally measured temperature. This is because the heating process takes place only from the barrel to the fluid, since the fluid near the barrel is not recirculated towards the bottom of the channel. In the above examples, the effect of viscous dissipation on the overall flow field was very small, while the effect of barrel temperature was large.

The comparisons between the numerically calculated and experimentally obtained die temperature and pressure are summarized in Table 1. Overall, the 3D (FEM) and 2D (FDM) models give close predictions of the die temperature and pressure.

4. CONCLUSIONS

A detailed numerical study of the three-dimensional transport processes associated with plastic extrusion in a single-screw extruder is carried out using a finite element scheme. The problem is complicated due to the non-Newtonian behavior of the fluid, variable properties and complex geometry of the extruder. Using the barrel moving formulation, which simplifies the simulation, the flow and temperature fields are computed for the self-wiping screw profile which is commonly used in extrusion systems. A marching scheme in the down-channel direction is used to simplify the calculations and provide an easy approach to include material property variations. Shear rate contours and heat transfer rates are also determined. It is found that a recirculating flow arises in the screw channel as fluid moves towards the die. This results in the hot fluid from near the barrel moving to the screw root and distorting the temperature profile. Simpler two-dimensional modeling is shown to be incapable of capturing this recirculation, indicating the need for a three-dimensional simulation.

The numerical results are also compared with experimental data obtained on an experimental single-screw extruder facility. Good agreement between the two is obtained, lending support to the present model and validating the various approximations made.

Acknowledgments—The authors acknowledge the support provided by the Center for Advanced Food Technology, NJ Commission of Science and Technology, for this work and the help of Dr A. H. Abib and R. V. Chiruvella in the preparation of the manuscript.

REFERENCES

1. Z. Tadmor and C. G. Gogos, *Principles of Polymer Processing*. Wiley, New York (1979).
2. H. S. Rowell and R. D. Finlayson, *Engineering* **114**, 606, (1922).
3. R. M. Griffith, Fully developed flow in screw extruders, *I & E C Fundam.* **1**(3), 181–187 (1962).
4. H. J. Zamodits and J. R. A. Pearson, Flow of polymer melts in extruders. Part i. The effect of transverse flow and of a superposed steady temperature profile, *Trans. Soc. Rheol.* **13**(3), 357–385 (1969).
5. C. Rauwendaal, Throughput-pressure relationships for power law fluids in single screw extruders, SPE ANTEC Tech. Pap. **31**, 30–33 (1985).
6. C. Karian, Power consumption for extrusion of non-Newtonian melt, SPE ANTEC Tech. Papers, **32**, 988–994 (1986).
7. E. Mitsoulis, J. Vlachopoulos and F. A. Mirza, Finite element analysis of flow through dies and extruder channels, SPE ANTEC Tech. Papers, **30**, 53–58 (1984).
8. B. Elbirli and J. T. Lindt, A note on the numerical treatment of the thermally developing flow in screw, *Polymer Engng Sci.* **24**(7), 482–487 (1984).
9. J. T. Lindt, Flow of a temperature dependent power-law fluid between parallel plates: an approximation for flow in a screw extruder, *Polymer Engng Sci.* **29**(7), 471–478 (1989).
10. J. T. Lindt, Mathematical modeling of melting of polymers in a single-screw extruder. A critical review, *Polymer Engng Sci.* **25**(10), 585–588 (1985).
11. R. T. Fenner, *Principles of Polymer Processing*. Chemical Publishing, New York (1979).
12. R. T. Fenner, Developments in the analysis of steady screw extrusion of polymers. *Polymer* **18**, 617–635 (1977).
13. E. E. Agur and J. Vlachopoulos. Numerical simulation of single-screw plasticating extruder, *Polymer Engng Sci.* **22**(17), 1084–1094 (1982).
14. A. Lawal and D. M. Kalyon, Incorporation of wall slip in non-isothermal modeling of single screw extrusion processing, 1st *Int. Conf. Transp. Phenom. Processing*, pp. 985–996. Technomic, Lancaster, PA (1993).
15. M. Gupta, T. Kown and Y. Jaluria, Multivariant finite element for three-dimensional simulation of viscous incompressible flows. *Int. J. Numer. Meth. Fluids* **14**, 557–585 (1992).
16. M. V. Karwe and Y. Jaluria, Numerical simulation of fluid flow and heat transfer in a single screw extruder for non-Newtonian fluids, *Numer. Heat Transfer* **17**, 167–190 (1990).
17. T. Sastrohartono, Y. Jaluria, and M. V. Karwe. Numerical coupling of multiple region simulations to study transport in a twin-screw extruder. *Numer. Heat Transfer* **25**, 541–557 (1994).
18. M. Esseghir and V. Sernas, A cam-driven probe for measurement of the temperature distribution in an extruder channel, SPE ANTEC Tech. Papers, 37, 54–57 (1991).
19. T. Sastrohartono, Finite element analysis of transport processes in single- and twin-screw extruders. Ph.D. Thesis, Rutgers—The State University of New Jersey, New Brunswick, NJ (1992).
20. L. E. Malvern, *Introduction to the Mechanics of a Continuous Medium*. Prentice-Hall, Englewood Cliffs, NJ (1969).
21. Y. Jaluria and K. E. Torrance, *Computational Heat Transfer*. Hemisphere, Washington, DC (1986).
22. A. J. Baker, *Finite Element Computational Fluid Mechanics*. Hemisphere, Washington, DC (1983).
23. S. S. Rao, *The Finite Element Method in Engineering*. Pergamon Press, Oxford (1989).
24. O. C. Zienkiewicz, *The Finite Element Method*. McGraw-Hill, London (1977).
25. M. Esseghir, An experimental investigation of the transport phenomena in single-and twin-screw extruders. Ph.D. Thesis, Rutgers—The State University of New Jersey, New Brunswick, NJ (1991).
26. M. L. Booy, Geometry of fully wiped twin-screw equipment. *Polymer Engng Sci.* **18**(12), 973–984 (1978).
27. M. L. Booy, Isothermal flow of viscous liquids in corotating twin screw devices. *Polymer Engng Sci.* **20**(18), 1220–1228 (1980).
28. B. K. Hwang Jr, Fluid flow studies in twin-screw extruders. Ph.D. Thesis, University of Delaware, DE (1982).
29. T. Sabol, Experiments in single-screw extruder. Masters Thesis, Rutgers—The State University of New Jersey, New Brunswick, NJ (1992).
30. T. Sabol, Personal communication, Rutgers University, New Brunswick, NJ (1991).
31. Y. Jaluria, T. H. Kwon and V. Sernas, Transport phenomena in food extrusion. Technical Report RU-TR-176-MAE-H, Department of Mechanical and Aerospace Engineering, Rutgers University, New Brunswick, NJ (1990).